Positron Scattering from Gas-Phase Beryllium and Magnesium: Theory, Recommended Cross Sections, and Transport Simulations

Cite as: J. Phys. Chem. Ref. Data **48**, 033103 (2019); https://doi.org/10.1063/1.5115353
Submitted: 13 May 2019 . Accepted: 17 June 2019 . Published Online: 24 July 2019

F. Blanco, G. García, R. P. McEachran, P. W. Stokes, R. D. White, and M. J. Brunger

Journal of Physical and Chemical Reference Data ARTICLE scitation.org/journal/jpr

Positron Scattering from Gas-Phase Beryllium and Magnesium: Theory, Recommended Cross Sections, and Transport Simulations

Cite as: J. Phys. Chem. Ref. Data 48, 033103 (2019); doi: 10.1063/1.5115353
Submitted: 13 May 2019 • Accepted: 17 June 2019 •
Published Online: 24 July 2019

F. Blanco,[1] G. García,[2] R. P. McEachran,[3] P. W. Stokes,[4] R. D. White,[4] and M. J. Brunger[5,a]

AFFILIATIONS

[1] Departamento de Estructura de la Materia Física Térmica y Electrónica, e IPARCOS, Universidad Complutense de Madrid, Plaza de Ciencias 1, E-28040, Madrid, Spain
[2] Instituto de Física Fundamental, CSIC, Serrano 113-bis, E-28006, Madrid, Spain
[3] Plasma Research Laboratory, RSPE, Australian National University, Canberra, ACT 0200, Australia
[4] College of Science and Engineering, James Cook University, Townsville, Queensland 4810, Australia
[5] College of Science and Engineering, Flinders University, GPO Box 2100, Adelaide, SA 5001, Australia

[a] **Author to whom correspondence should be addressed:** michael.brunger@flinders.edu.au

ABSTRACT

Results from the application of our optical potential and relativistic optical potential models to positron scattering from gas-phase beryllium (Be) and magnesium (Mg) are presented. Specifically, total cross sections and integral cross sections for the elastic, positronium formation, summed discrete electronic-state excitation, and ionization scattering processes are reported for both species and over an extended incident positron energy range. Where possible, these results are compared against the existing theoretical and experimental data, although it must be noted here that no current measurements are yet available for Be and those that are available for Mg are largely restricted to the total cross section. Nonetheless, on the basis of that comparison, recommended cross section datasets, for all the aforementioned cross sections, are formed. Those recommended cross section data are subsequently employed in a Boltzmann equation analysis to simulate the transport of positrons, under the influence of an applied (external) electric field, through the background Be and Mg gases. Note that relativistic optical potential results for the elastic momentum transfer cross section are also reported, to allow us to account for anisotropy effects in our transport simulations. Finally, our positron simulation results for quantities such as the ionization rate coefficients and flux and bulk drift velocities are compared with the corresponding electron transport results with significant differences being observed.

Published by AIP Publishing on behalf of the National Institute of Standards and Technology. https://doi.org/10.1063/1.5115353

Key words: beryllium; magnesium; positron scattering cross sections; positron transport; recommended cross sections.

CONTENTS

List of Tables

List of Figures

1. Introduction

Previous investigations into positron scattering from beryllium (Be) and magnesium (Mg) have been limited in terms of either the types of processes considered (i.e., elastic, discrete inelastic, positronium formation, ionization, and the total cross section) and/or the energy range being studied. From an experimental perspective, the absence of a section on Be in the two recent positron–atom scattering reviews[1,2] is strong evidence for no such data existing in the literature. This situation, however, arises from the real practical challenges in working with Be and in trying to establish a source of gas-phase Be-atoms. On the other hand, the situation is somewhat improved in terms of theoretical studies into this scattering system. In particular, we note the elastic integral cross section (ICS) results from Bromley *et al.*,[3] Mitroy and Ivanov,[4] Reid and Wadehra,[5] and Poveda *et al.*[6] Note that below the positronium formation channel threshold energy (E_{Ps} = 2.522 eV) in Be, those elastic ICSs are equivalent to the total scattering cross section (TCS). Further note that currently it appears that no theoretical results for the positronium formation, discrete inelastic, and ionization channels are available for positron–Be scattering. Rectifying this deficiency, through application of our optical potential (OP) and relativistic optical potential (ROP) computational methods, thus forms one rationale for this work. In regard to positron–Mg scattering, experimental data, largely from the group that was based at Wayne State University, can be found in the literature.[7,8] Most of that data relates to the TCS, although a preliminary result for the positronium formation ICS was published in the work of Surdutovich *et al.*[9] However, in their review, Ratnavelu *et al.*[2] declined to use that preliminary data in order to form a recommended positronium formation cross section and as a consequence we do not consider it further. Similar to that just described above for Be, theoretical elastic ICSs for positron–Mg scattering are also available from Bromley *et al.*,[3] Mitroy and Ivanov,[4] Reid and Wadehra,[5] and Poveda *et al.*[6] In this case, those elastic ICSs equate to the TCS below 0.846 eV, the positronium formation threshold energy of Mg. In addition, there are also elastic ICS theoretical results from Mitroy *et al.*,[10] Savage *et al.*[11] [a single-center convergent close coupling (CCC) result], and Utamuratov *et al.*[12] (a two-center CCC result). Quite a significant degree of theoretical endeavor is also apparent in studying the positronium formation channel. This includes the results from Gribakin and King,[13] Hewitt *et al.*,[14] Chang and Zhou,[15] and Utamuratov *et al.*[12] However, the agreement between those calculations for that channel is rather poor. Finally, we note that the only previous ionization ICS for the positron–Mg system is from Uramuratov *et al.*,[12] while there are no current results for the discrete inelastic channels. In order to try and better understand the discrepancies between the existing Mg calculations, and add to the database where only one or no computational result is currently available, we have also applied our OP and ROP methods to this scattering system. This forms another important rationale for the current investigation.

There has been quite a bit of historical interest in comparing electron and positron scattering cross section results, with significant experimental work in this respect being undertaken at Yamaguchi University (e.g., Refs. 16 and 17) and the University of Trento.[18–20] The rationale, in part, behind those investigations was to see at what energy the electron and positron results (usually at the TCS level) converged to the same values. Typically, that convergence was thought to occur once the exchange interaction (in electron scattering) and positronium formation (in positron scattering) became so small that they could be neglected. At that point, the positron and electron interactions, from a given target, were considered to be largely identical so that their cross sections converged. This was found to be the case, to within the uncertainties on the data, in many examples,[21] although the energy at which the cross section values merged was very target specific.[16–20] Note that while the polarization interaction in both the electron and positron scattering cases does act

the same, due to the different charges the static interaction, in principle, remains different at all energies. We therefore also wished to investigate this effect with our OP and ROP calculations in both Be and Mg, drawing on our recent electron–Be[22] and electron–Mg[23] results in order to do so. Furthermore, and we believe this is the first time such a study has been undertaken, we intend to use our cross section data for electron and positron scattering in order to simulate their transport characteristics through background Be and Mg gases, under the influence of an applied (external) electric field, and to investigate any similarities or differences in their behavior across a range of reduced electric fields (E/n_0, where E = electric field strength and n_0 = number density).

The structure of the remainder of this paper is as follows: In Sec. 2, we provide details of our OP and ROP calculations, while in Sec. 3 these results are compared and discussed against those, for both Be and Mg, which are currently available in the literature. On the basis of that comparison, in Sec. 4, we formulate the recommended data for those species for total scattering, elastic scattering, positronium formation, the sum of all the discrete inelastic channels, and ionization. Using these recommended positron cross section sets, and corresponding data (where appropriate) for electron scattering,[22,23] in Sec. 5, the results from our Boltzmann equation analysis of positron and electron transport in Be and Mg are presented. Brief details of our simulation methodology are also given in Sec. 5. Finally, in Sec. 6, some conclusions from this investigation are outlined.

2. Theoretical Details

In this section, we provide some brief details with respect to our current OP and ROP theoretical methods and their application to positron (e^+) scattering processes.

TABLE 1. The present theoretical OP results ($\times 10^{-16}$ cm^2) for positron scattering from beryllium

Energy (eV)	Elastic ICS ($\times 10^{-16}$ cm^2)	Ps formation ($\times 10^{-16}$ cm^2)	Excitation ($\times 10^{-16}$ cm^2)	Direct ionization ICS ($\times 10^{-16}$ cm^2)	Total ($\times 10^{-16}$ cm^2)
0.1	383.6	0	0	0	383.6
0.15	296.8	0	0	0	296.8
0.2	242.76	0	0	0	242.76
0.3	177.8	0	0	0	177.8
0.4	141.96	0	0	0	141.96
0.5	119.84	0	0	0	119.84
0.7	93.8	0	0	0	93.8
1	72.8	0	0	0	72.8
1.5	53.48	0	0	0	53.48
2	42	0	0	0	42
3	28.84	0	0	0	28.84
4	21.952	0.5208	0	0	22.4728
5	15.904	6.636	0	0	22.54
7	10.92	11.284	3.556	0	25.76
10	9.716	7.084	9.06808	0.14392	26.012
15	8.708	4.704	6.944	3.5	23.856
20	7.896	4.508	4.844	4.872	22.12
30	6.468	4.284	3.388	4.76	18.9
40	4.844	3.108	2.772	4.228	14.952
50	3.612	1.904	2.408	3.752	11.676
70	2.408	0.728	1.96	3.052	8.148
100	1.68	0.224	1.554	2.422	5.88
150	1.1564	0.056	1.1732	1.8228	4.2084
200	0.8932	0.028	0.9436	1.4784	3.3432
300	0.6272	0	0.6888	1.0864	2.4108
400	0.4844	0	0.546	0.8652	1.8984
500	0.3976	0	0.4564	0.7252	1.582
700	0.2912	0	0.3472	0.5488	1.1872
1000	0.20944	0	0.2576	0.4088	0.87584
2000	0.10612	0	0.14672	0.22288	0.47572
3000	0.07028	0	0.10276	0.15372	0.32676
4000	0.05292	0	0.08036	0.11816	0.25144
5000	0.04256	0	0.06608	0.09576	0.2044
7000	0.03108	0	0.049	0.06916	0.14924
10000	0.023212	0	0.03528	0.049	0.107492

Published by AIP Publishing on behalf of the National Institute of Standards and Technology.

2.1. OP

Our OP method is based on a local complex potential representing the atomic scattering center, according to the following equation:

$$V(r) = V_s(r) + V_p(r) - iV_a(r), \quad (1)$$

where $V_s(r) + V_p(r)$ is the real or elastic scattering part of the OP and $iV_a(r)$ is the imaginary absorption potential, accounting for the inelastic scattering channels. $V_s(r)$ represents the static potential, describing the interaction between the positron and the atomic charge density, and is repulsive in the case of positrons. We formulate this on a derivation of the Hartree-Fock atomic wavefunctions, analogous to the work of Reid and Wadehra.[24] $V_p(r)$ represents the polarization potential which accounts for the target electron cloud deformation during the collision and is therefore dependent on its atomic polarizability. We have shown in previous studies with oxygen (O) containing molecular targets how sensitive low energy elastic positron scattering is to the accuracy on the description of this term.[25,26] In that case, we used the sum of a dipole and quadrupole potential calculated with the polarized-orbital method, by determining the first-order corrections of the atomic orbitals due to a fixed charge field.[27] For O, the dipole and quadrupole polarized orbital potential of Ne (accurate against measurement[28]) was scaled according to the procedure described in the work of Chiari *et al.*[26] A similar procedure is not currently available for Be and Mg so we decided to use the energy dependent polarization potential quite recently proposed by Reid and Wadehra.[5] $V_a(r)$ describes the "absorption" processes, i.e., the inelastic processes of excitation, ionization, and positronium formation (Ps), and require careful treatment. We use a scheme modified from that proposed by Reid and Wadehra,[24] assuming that the target electrons can be considered as a quasifree electron cloud with which the incoming particles undergo binary collisions. The threshold energy is carefully designed to include Ps formation.

Our recent improvements to the treatment of Ps formation are outlined in detail previously.[29] In brief, we use an energy dependent threshold $\Delta(E)$ coinciding with the well-known Ps formation threshold of $\Delta_p = I - 6.8$ eV (where I = ionization threshold), for lower energies, and the lowest optically allowed excitation transition Δ for higher impact energies by assuming a smooth transition in threshold energy, from low to high impact energy, which follows the expression

$$\Delta(E) = \Delta - \frac{(\Delta - \Delta_p)}{\left[1 + \left(\frac{E}{3I} - 1\right)^2\right]}. \quad (2)$$

Hence, we used $\Delta = 5.28$ eV for Be, but in the particular case of Mg instead of the lowest optically allowed excitation transition we employed $\Delta = 2.71$ eV, which corresponds to a forbidden transition which, probably due to the strong configuration mixing present in Mg, contributes notably to the emission spectrum.[23]

The present OP results for positron scattering from Be are summarized in Table 1 and Fig. 1, while those for positron scattering from Mg are summarized in Table 2 and Fig. 2.

2.2. ROP details

The theoretical procedures used here to describe the elastic and inelastic scattering of positrons from beryllium and magnesium atoms is based upon the ROP method of Chen *et al.*,[30] hereafter referred to as Paper I. This OP method is based upon an approximate solution of the relativistic close-coupling equations. Only a brief discussion of the overall method will be given here, and the reader is referred to Ref. I for details.

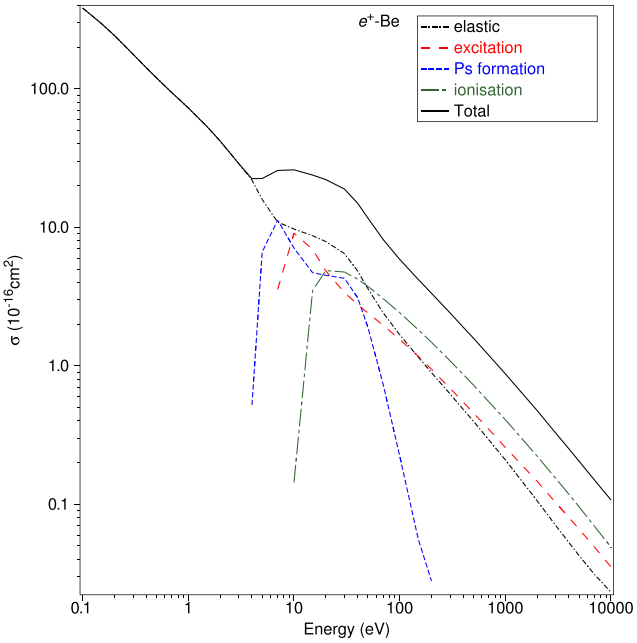

FIG. 1. The present OP integral and total cross section results for positron scattering from beryllium. See the legend in the figure for the processes considered.

The scattering of the incident positrons, with wavenumber k, by beryllium and magnesium atoms is described by the integral equation formulation of the partial wave Dirac-Fock scattering equations. In the ROP method, these equations can be expressed in matrix form as

$$\begin{pmatrix} F_\kappa(r) \\ G_\kappa(r) \end{pmatrix} = \begin{pmatrix} v_1(kr) \\ v_2(kr) \end{pmatrix} + \frac{1}{k}\int_0^r dx\, G(x,r) \times \left[U(r)\begin{pmatrix} F_\kappa(r) \\ G_\kappa(r) \end{pmatrix} - iU_a(r)\begin{pmatrix} F_\kappa(r) \\ G_\kappa(r) \end{pmatrix}\right], \quad (3)$$

where the local potential $U(r)$ is given by the sum of the static and local polarization potentials, i.e.,

$$U(r) = U_{st}(r) + U_{pol}(r). \quad (4)$$

Here, we used the procedure outlined by Bartschat *et al.*,[31,32] whereby the real part of the OP was replaced by a local polarization potential based upon a polarized-orbital method of McEachran *et al.*[27,33] The static potentials were determined in the usual manner from the Dirac-Fock orbitals of the atoms. The polarization potentials $U_{pol}(r)$ in Eq. (4) comprised the sum of the first 11 multipole polarization potentials using the polarized-orbital method of McEachran *et al.*[27] This potential was then augmented by an additional potential obtained by an extrapolation to an infinite number of multipoles as detailed in the work of McEachran *et al.*[33] In Eq. (3), the nonlocal potential $U_a(r)$ denotes the imaginary part of the OP and, in turn, describes the

Published by AIP Publishing on behalf of the National Institute of Standards and Technology.

TABLE 2. The present theoretical OP results ($\times 10^{-16}$ cm^2) for positron scattering from magnesium

Energy (eV)	Elastic ICS ($\times 10^{-16}$ cm^2)	Ps formation ($\times 10^{-16}$ cm^2)	Excitation ($\times 10^{-16}$ cm^2)	Direct ionization ICS ($\times 10^{-16}$ cm^2)	Total ($\times 10^{-16}$ cm^2)
0.1	226.52	0	0	0	226.52
0.15	237.16	0	0	0	237.16
0.2	249.76	0	0	0	249.76
0.3	268.52	0	0	0	268.52
0.4	271.04	0	0	0	271.04
0.5	260.12	0	0	0	260.12
0.7	222.6	0	0	0	222.6
1	171.92	0	0	0	171.92
1.5	120.96	0	0	0	120.96
2	86.52	7.448	0	0	93.968
3	35.84	35.042	1.638	0	72.52
4	26.516	20.16	16.8	0	63.476
5	23.296	10.388	24.332	0	58.016
7	20.412	6.16	25.76	0	52.332
10	18.648	6.244	20.496	2.94	48.328
15	17.276	7.476	12.516	7.812	45.08
20	16.436	8.596	9.912	8.232	43.176
30	13.272	7.336	7.84	7.336	35.784
40	9.8	4.116	6.776	6.44	27.132
50	7.728	2.268	6.02	5.768	21.784
70	5.656	0.812	5.04	4.788	16.296
100	4.228	0.28	4.088	3.892	12.488
150	3.08	0.084	3.164	3.052	9.38
200	2.4668	0.056	2.6096	2.5424	7.6748
300	1.8144	0	1.9852	1.9628	5.7624
400	1.456	0	1.6212	1.6268	4.704
500	1.2376	0	1.386	1.414	4.0376
700	0.9576	0	1.0976	1.1312	3.1892
1000	0.7308	0	0.8652	0.8932	2.492
2000	0.42	0	0.5628	0.5516	1.5344
3000	0.2968	0	0.4396	0.4088	1.1452
4000	0.22988	0	0.3724	0.3276	0.92988
5000	0.18732	0	0.32452	0.27468	0.78652
7000	0.13636	0	0.26152	0.20888	0.60676
10000	0.09688	0	0.20664	0.15456	0.45808

absorption of the incident flux into the inelastic channels and thereby describes both excitation and ionization processes. This potential is given by a sum and integration over the bound and continuum states of the atom [see Sec. 2.2.1 as well as Eq. (21b) of Ref. I for details].

Finally, in Eq. (3), $F_\kappa(r)$ and $G_\kappa(r)$ are the large and small components of the complex scattering wavefunctions, while the functions $v_1(kr)$ and $v_2(kr)$ are the corresponding free particle wavefunctions and are given in terms of Riccati-Bessel functions. $G(r, x)$ is the free particle Green's function which can be expressed in matrix form in terms of the Riccati-Bessel and Riccati-Neumann functions [see Eqs. (23) and (24a,b) of Ref. I for details]. The subscript κ on the scattering wavefunctions is the relativistic angular momentum quantum number of the incident positron. It is related to the corresponding orbital angular momentum quantum number l according to $\kappa = -l - 1$ when $j = l + \frac{1}{2}$ (spin-up) and $\kappa = l$ when $j = l - \frac{1}{2}$ (spin-down), where j is the total angular momentum quantum number of the incident positron.

The large component of the complex scattering wavefunction is given asymptotically by

$$F_\kappa(r)_{r\to\infty} \longrightarrow \sin\left(kr - \frac{l\pi}{2}\right) + T_l^{\pm}(k)\exp\left(ikr - \frac{l\pi}{2}\right), \quad (5)$$

where $T_l^{\pm}(k)$ are the complex T-matrix elements. These T-matrix elements can be expressed in terms of the complex phase shifts $\eta_l^{\pm}(k)$ according to

$$T_l^{\pm}(k) = \frac{1}{2i}\left[\exp\left(2i\eta_l^{\pm}(k)\right) - 1\right], \quad (6)$$

where the real and imaginary parts of the phase shifts are given by

$$\eta_l^{\pm}(k) = \delta_l^{\pm}(k) + i\,\gamma_l^{\pm}(k). \quad (7)$$

Published by AIP Publishing on behalf of the National Institute of Standards and Technology.

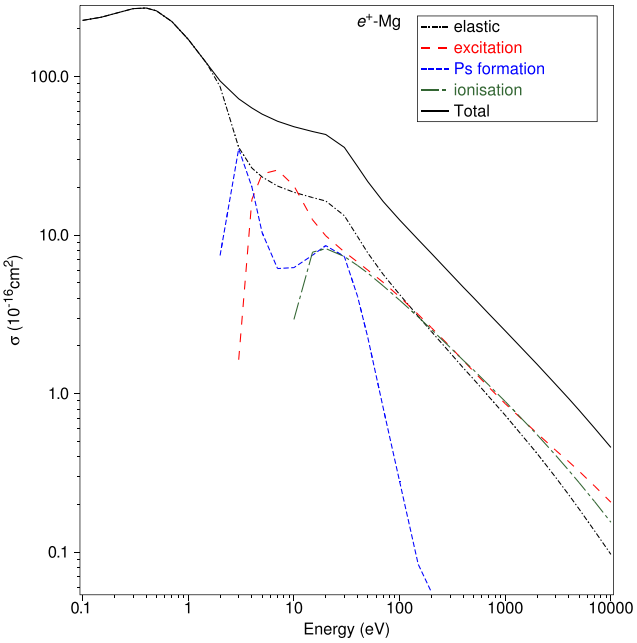

FIG. 2. The present OP integral and total cross section results for positron scattering from magnesium. See the legend in the figure for the processes considered.

Here, the superscript + refers to "spin-up," while the superscript − refers to "spin-down." The integrated elastic cross section is then given, in terms of these real and imaginary parts of the phase shifts, by

$$\sigma^{\mathrm{el}}(k^2) = \frac{2\pi}{k^2}\sum_{l=0}^{\infty}\{(l+1)\exp(-2\gamma_l^+)\,[\cosh 2\gamma_l^+ - \cos 2\delta_l^+] + l\exp(-2\gamma_l^-)[\cosh 2\gamma_l^- - \cos 2\delta_l^-]\}, \quad (8)$$

while the total inelastic or absorption cross section is given by

$$\sigma^{\mathrm{inel}}(k^2) = \frac{\pi}{k^2}\sum_{l=0}^{\infty}\{(l+1)\,[1-\exp(-4\gamma_l^+)] + l\,[1-\exp(-4\gamma_l^-)]\}. \quad (9)$$

2.2.1. Positronium formation

Here, positronium formation was simulated using the method given in the work of McEachran and Stauffer[34] which, in turn, is a modification of that originally suggested by Reid and Wadehra.[24,35] In this method, the Ps formation cross section is calculated by first determining the direct ionization cross section and then the comparable cross section when the ionization thresholds are reduced by 6.8 eV, the binding energy of the ground state of positronium. The Ps formation cross section is then taken to be the difference between these two cross sections. Similarly, Ps formation in an excited state with principle quantum number n can be simulated by reducing the ionization thresholds by $6.8/n^2$ eV. Here, we included the $n = 2$, 3, and 4 excited states of positronium.

Any method for simulating rather than directly calculating Ps formation will contain one or more adjustable parameters. In the method of McEachran and Stauffer,[34] there is just one adjustable parameter which is chosen according to where the Ps formation cross section effectively vanishes. For the noble gases, for which there are many experimental measurements, this parameter was chosen to be 120 + E_{ion} eV. For two-electron systems, there are hardly any experimental measurements of Ps formation, except for helium. Consequently, based upon the measurements of Murtagh *et al.*,[36] the cutoff here was chosen to be 200 + E_{ion} eV. It should be noted that in the method of McEachran and Stauffer,[34] this adjustable parameter influences the asymptotic behavior of the Ps formation cross section but has very little influence on its peak value.

2.2.2. The absorption potential

For beryllium, the following 10 bound excited states were included in $U_a(r)$, namely, $np^{1,3}P^o$ with n = 2–6 in order to simulate excitation processes. Similarly, for magnesium, the 10 bound excited states included in $U_a(r)$ were $np^{1,3}P^o$ with n = 3–7. Also included in $U_a(r)$, for both beryllium and magnesium, were all continuum states with the orbital angular momentum given by l_c = 0, 1, 2, 3, and 4 in order to simulate ionization processes. The integration over the continuum states in the absorption potential was approximated by using Gauss-Legendre integration with 16–20 points. In a relativistic close-coupling expansion, it is necessary to couple the total angular momentum of the electron in the excited state (bound or continuum) to the total angular momentum of the incident positron in order to obtain the total angular momentum J of the positron-atom system. This total angular momentum J is then conserved during the collision process. Under the above circumstances, this gave rise to a maximum of 30 excitation channels and 84 ionization channels in $U_a(r)$ for both beryllium and magnesium.

The present ROP results for positron scattering from Be are summarized in Table 3 and Fig. 3, while those for positron scattering from Mg are summarized in Table 4 and Fig. 4.

3. Data Comparison

In Fig. 5, we plot the available data[3–6] for positron scattering from Be, along with our OP and ROP results, for elastic scattering, positronium formation, the sum over discrete electronic-state excitation, ionization, and total scattering. There are several general observations we can make in relation to Fig. 5. First, as noted earlier, there are no experimental results against which we can compare the data from the theoretical computations. In addition, for positronium formation, discrete electronic-state excitation, and ionization only, the present OP and ROP results are now available. Considering first the elastic ICS at very low energies, then with the exception of our ROP calculation, which is too high in magnitude, the results from Poveda *et al.*,[6] Bromley *et al.*,[3] Mitroy and Ivanov,[4] and Reid and Wadehra[5] are all in quite good accord. Note that in the work of McEachran *et al.*,[22,23] we had previously described that the ROP method at lower energies was not expected to be as accurate as close coupling results, and this point is reinforced in Fig. 5(a) although now for positron scattering. At energies above about 1 eV, all the available theoretical results, in their energy regions of overlap, are in very good agreement. In particular, we highlight the excellent accord between our OP and ROP results up to 5000 eV. For the positronium formation [Fig. 5(b)], sum over discrete electronic-state excitation [Fig. 5(c)], and ionization [Fig. 5(d)], our OP and ROP calculations

Published by AIP Publishing on behalf of the National Institute of Standards and Technology.

TABLE 3. A selection of the present ROP results ($\times 10^{-16}$ cm^2) for positron scattering from beryllium. Note that the acronym MTCS denotes the momentum transfer cross section, used in Sec. 5 in the transport simulations (see later)

Energy (eV)	Elastic ICS ($\times 10^{-16}$ cm^2)	MTCS ($\times 10^{-16}$ cm^2)	Excitation ($\times 10^{-16}$ cm^2)	Direct ionization ICS ($\times 10^{-16}$ cm^2)	Ps formation ($\times 10^{-16}$ cm^2)	Total ($\times 10^{-16}$ cm^2)
0.0000	3514.0300	3514.0300	0.0000	0.0000	0.0000	3514.0300
0.0100	2268.8500	2297.7600	0.0000	0.0000	0.0000	2268.8500
0.0200	1650.8800	1677.6800	0.0000	0.0000	0.0000	1650.8800
0.0400	1054.0500	1072.1100	0.0000	0.0000	0.0000	1054.0500
0.0600	764.9700	774.9200	0.0000	0.0000	0.0000	764.9700
0.0800	595.3500	598.4400	0.0000	0.0000	0.0000	595.3500
0.1200	406.5100	398.6800	0.0000	0.0000	0.0000	406.5100
0.1600	305.1700	289.0000	0.0000	0.0000	0.0000	305.1700
0.2500	192.9800	163.8500	0.0000	0.0000	0.0000	192.9800
0.3500	137.3500	99.8200	0.0000	0.0000	0.0000	137.3500
0.4500	108.0800	66.1500	0.0000	0.0000	0.0000	108.0800
0.5500	90.4100	46.7000	0.0000	0.0000	0.0000	90.4100
0.6570	77.9100	34.1600	0.0000	0.0000	0.0000	77.9100
0.9000	60.6700	20.3800	0.0000	0.0000	0.0000	60.6700
1.2000	48.2400	13.9800	0.0000	0.0000	0.0000	48.2400
1.8000	34.0900	9.4300	0.0000	0.0000	0.0000	34.0900
2.6000	24.4086	6.7824	0.0000	0.0000	0.1183	24.5269
2.7000	23.5449	6.5248	0.0000	0.0000	0.3710	23.9159
2.8000	22.7218	6.2754	0.0164	0.0000	0.6707	23.4089
2.9000	21.9538	6.0409	0.0237	0.0000	0.9898	22.9673
3.0000	21.2345	5.8202	0.0281	0.0000	1.3140	22.5766
3.4000	18.7751	5.0627	0.0359	0.0000	2.5381	21.3491
4.0000	16.0382	4.2179	0.0379	0.0000	3.9781	20.0541
5.2000	12.5801	3.1530	0.0346	0.0000	5.6504	18.2651
5.4000	12.7283	3.3402	3.3287	0.0000	5.3211	21.3782
6.2000	13.0475	3.3597	8.0038	0.0000	4.8584	25.9097
8.0000	12.2323	2.3016	13.6204	0.0000	4.3058	30.1585
8.2000	12.1233	2.2056	13.1853	0.0000	4.3084	29.6170
9.4000	11.5017	1.7352	16.2071	0.0095	4.5816	32.2999
9.6000	11.3777	1.6695	16.4122	0.0619	4.6119	32.4638
10.0000	11.1255	1.5500	16.7163	0.2194	4.6096	32.6709
12.0000	9.9804	1.1324	17.7046	1.1899	4.1247	32.9996
14.0000	8.9622	0.8930	18.0313	1.9683	3.4726	32.4344
18.0000	7.3501	0.6553	17.7249	2.8339	2.3905	30.2995
22.0000	6.2279	0.5447	17.4088	3.1567	1.6629	28.4563
26.0000	5.3772	0.4821	16.6850	3.2196	1.2002	26.4821
30.0000	4.7285	0.4420	15.8581	3.1633	0.8980	24.6479
35.0000	4.1232	0.4066	14.9840	3.0242	0.6539	22.7853
40.0000	3.6695	0.3791	14.2927	2.8604	0.4965	21.3190
50.0000	3.0272	0.3347	13.1214	2.5389	0.3177	19.0052
60.0000	2.5890	0.2981	12.0010	2.2616	0.2239	17.0755
80.0000	2.0283	0.2398	10.0366	1.8418	0.1292	14.0359
100.0000	1.6842	0.1963	8.5716	1.5499	0.0813	11.8871
110.0000	1.5566	0.1788	8.0767	1.4364	0.0706	11.1403
120.0000	1.4294	0.1495	7.5859	1.4576	0.0686	10.5415
140.0000	1.2578	0.1271	6.8041	1.2910	0.0444	9.3972
170.0000	1.0703	0.1023	5.9139	1.1042	0.0207	8.1091
190.0000	0.9753	0.0900	5.4391	1.0085	0.0097	7.4325
200.0000	0.9344	0.0848	5.2269	0.9665	0.0051	7.1329
275.0000	0.7151	0.0583	4.0722	0.7381	0.0000	5.5254
425.0000	0.4937	0.0347	2.6654	0.5038	0.0000	3.6629

Published by AIP Publishing on behalf of the National Institute of Standards and Technology.

TABLE 3. (*Continued.*)

Energy (eV)	Elastic ICS ($\times 10^{-16}$ cm^2)	MTCS ($\times 10^{-16}$ cm^2)	Excitation ($\times 10^{-16}$ cm^2)	Direct ionization ICS ($\times 10^{-16}$ cm^2)	Ps formation ($\times 10^{-16}$ cm^2)	Total ($\times 10^{-16}$ cm^2)
650.0000	0.3417	0.0205	1.7082	0.3433	0.0000	2.3932
850.0000	0.2699	0.0145	1.2364	0.2671	0.0000	1.7734
1000.0000	0.2336	0.0116	1.0098	0.2286	0.0000	1.4720
1500.0000	0.1619	0.0064	0.6119	0.1547	0.0000	0.9285
2000.0000	0.1243	0.0041	0.4192	0.1152	0.0000	0.6587
2500.0000	0.1010	0.0029	0.3109	0.0905	0.0000	0.5025
3000.0000	0.0851	0.0021	0.2427	0.0736	0.0000	0.4014
4000.0000	0.0649	0.0013	0.1628	0.0520	0.0000	0.2798
5000.0000	0.0525	0.0009	0.1186	0.0389	0.0000	0.2100

are in a reasonable qualitative accord although some differences in the magnitudes of the cross sections are noted. Of particular interest in Fig. 5(c) is a near-threshold structure that can be ascribed to excitation of the 2^3P state of Be. In a nonrelativistic calculation, excitation of this state could only be via electron exchange, which is not available in positron scattering, and so one might *a priori* expect its cross section to be zero. However, in a relativistic framework (such as in our ROP results), this is not the case, due to configuration mixing, and although the interaction is quite weak, it will be nonzero as is shown in Fig. 5(c). Finally, we consider the TCS of Fig. 5(d). Most of the comments we made earlier in relation to the elastic ICS are equally valid here, except for the existence of a secondary maximum in a structure in the TCS at around 20 eV (seen in both our OP and ROP results). This feature in Fig. 5(d) is not due to the existence of a resonance, rather if reflects the strong opening for the lowest-lying dipole-allowed 2^1P state in Be.

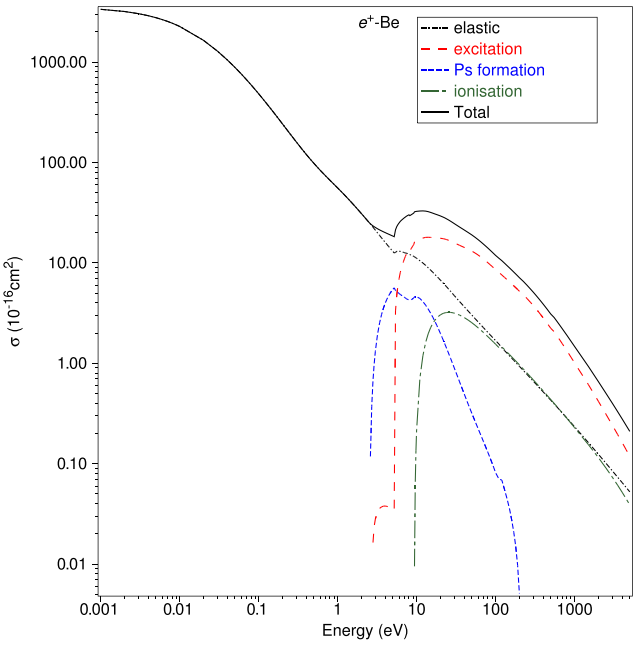

FIG. 3. The present ROP integral and total cross section results for positron scattering from beryllium. See the legend in the figure for the processes considered.

A similar comparison to that just given, but now for positron–Mg scattering, is made for the same scattering processes in Fig. 6. In this case, however, at the TCS level [Fig. 6(e)], we at least have experimental results from the Wayne State University group[7–9] which are embodied in the recommended data from Ratnavelu *et al.*[2] That data predicts a strong low-energy resonance feature, which is well reproduced by the theoretical results from the computations of Poveda *et al.*,[6] Mitroy *et al.*,[10] and the CCC[12] but not by our ROP or the results of Bromley *et al.*[3] Indeed, to within the ±20% data uncertainty cited by Ratnavelu *et al.*,[2] the level of accord between their recommended data and the CCC, over the common energy regime, is excellent [see Fig. 6(e)]. Note that for incident positron energies greater than about 20 eV, we highlight the very good level of agreement between our OP and ROP calculations and the CCC. This augurs very well for constructing a recommended higher energy TCS for positron–Mg scattering (see Sec. 4). Much of what we have just noted for the TCS is also valid for the elastic ICS [Fig. 6(a)], and so we do not discuss it further here. Considering Fig. 6(b), for the positronium formation ICS, we find theoretical results from Gribakin *et al.*,[13] Hewitt *et al.*,[14] Chang and Zhou,[15] the CCC,[12] and our OP and ROP calculations. It is clear from this figure [Fig. 6(b)] that there is quite a spread in the ICS magnitudes for this process, although with the exception of the Hewitt *et al.*[14] result, which is quasi-isotropic, the qualitative energy dependence of all the theories is quite similar. One interesting observation from Fig. 6(d) is that both our OP and ROP calculations predict the positronium formation cross section to persist to somewhat higher energies than that found in the 2-center CCC result.[12] In the case of He, the eigen 2-electron system (both Be and Mg can be considered as quasi-2-electron systems[22,23]), Ratnavelu *et al.*[2] recommended a positronium formation cross section, based on measurements, that persists out to about 200 eV. This energy range in He is more consistent, in this case, with the present OP and ROP computations than that from the CCC for Mg: In Fig. 6(c), we only have the OP and ROP results available for the ICSs for the sum over all discrete electronic-state excitations. Here, we note that our OP method has a problem[23] in that there is still an uncertainty as to which excitation threshold (3^3P or 3^1P state) energy is the appropriate one to employ (see Sec. 2). This arises as while the 3^3P transition is supposed to be forbidden, it is in fact optically observed in Mg. As a consequence, at this time

TABLE 4. A selection of the present ROP results ($\times 10^{-16}$ cm^2) for positron scattering from magnesium

Energy (eV)	Elastic ICS ($\times 10^{-16}$ cm^2)	MTCS ($\times 10^{-16}$ cm^2)	Excitation ($\times 10^{-16}$ cm^2)	Direct ionization ICS ($\times 10^{-16}$ cm^2)	Ps formation ($\times 10^{-16}$ cm^2)	Total ($\times 10^{-16}$ cm^2)
0.0000	695.5280	695.5280	0.0000	0.0000	0.0000	695.5280
0.0010	732.1410	745.4850	0.0000	0.0000	0.0000	732.1410
0.0800	463.6440	510.4020	0.0000	0.0000	0.0000	463.6440
0.1200	389.8210	408.8210	0.0000	0.0000	0.0000	389.8210
0.2000	311.3940	270.7770	0.0000	0.0000	0.0000	311.3940
0.2770	273.5100	189.3430	0.0000	0.0000	0.0000	273.5100
0.3400	252.2920	146.1530	0.0000	0.0000	0.0000	252.2920
0.4200	229.8870	110.4930	0.0000	0.0000	0.0000	229.8870
0.5000	209.8140	88.0610	0.0000	0.0000	0.0000	209.8140
0.6500	176.9180	64.2350	0.0000	0.0000	0.0000	176.9180
0.8750	138.7268	46.3253	0.0000	0.0000	0.4688	139.1956
0.9000	134.8134	44.7053	0.0000	0.0000	1.0150	135.8284
1.2000	97.2886	29.8558	0.0000	0.0000	8.7145	106.0031
1.4000	81.2173	23.7729	0.0000	0.0000	12.5755	93.7928
1.6000	69.7110	19.5057	0.0000	0.0000	15.4744	85.1854
2.0000	54.7187	14.1248	0.0000	0.0000	19.2659	73.9846
2.4000	45.5362	10.9924	0.0000	0.0000	21.3680	66.9042
2.8000	39.3450	8.9747	0.0678	0.0000	22.4843	61.8971
2.9000	38.1001	8.5771	0.0955	0.0000	22.6591	60.8547
3.2000	34.8979	7.5600	0.1420	0.0000	23.0410	58.0809
3.8000	30.1580	6.0746	0.1796	0.0000	23.3413	53.6789
4.2000	27.8007	5.3484	0.1902	0.0000	23.3273	51.3182
4.4000	27.6535	5.3987	2.5881	0.0000	21.6394	51.8810
4.6000	27.7982	5.5302	4.6974	0.0000	20.2001	52.6957
5.2000	26.6429	4.9959	8.8294	0.0000	17.8467	53.3190
6.4000	24.3225	3.7677	14.2539	0.0000	15.2958	53.8723
7.8000	22.0605	2.7576	17.9762	0.0505	14.6376	54.7249
8.0000	21.7609	2.6453	18.3502	0.1683	14.5144	54.7937
8.2000	21.4631	2.5397	18.6669	0.3160	14.3710	54.8171
10.0000	18.9303	1.8302	19.8088	1.9252	12.8590	53.5232
12.0000	16.6769	1.3834	20.2225	3.3747	11.1402	51.4143
14.0000	14.8845	1.1173	20.4804	4.3527	9.6210	49.3386
18.0000	12.1604	0.8360	19.7662	5.3781	7.4452	44.7499
22.0000	10.3012	0.7044	18.8894	5.7417	5.9063	40.8387
30.0000	7.9671	0.5867	17.6104	5.7117	3.9757	35.2649
40.0000	6.2703	0.5206	15.8525	5.2545	2.7640	30.1414
45.0000	5.6913	0.4982	14.9474	5.0007	2.3342	27.9737
55.0000	4.8369	0.4573	13.3604	4.5213	1.7346	24.4532
65.0000	4.2345	0.4184	12.0858	4.1166	1.3486	21.7855
85.0000	3.4404	0.3537	10.2050	3.5090	0.8640	18.0184
100.0000	3.0376	0.3100	9.1515	3.2093	0.6370	16.0354
120.0000	2.6544	0.2706	8.2710	2.8767	0.4197	14.2218
140.0000	2.3744	0.2409	7.4477	2.6107	0.2636	12.6963
160.0000	2.1600	0.2178	6.7563	2.3928	0.1553	11.4644
180.0000	1.9896	0.1992	6.1625	2.2108	0.0787	10.4417
190.0000	1.9168	0.1912	5.8955	2.1304	0.0489	9.9917
200.0000	1.8507	0.1840	5.6460	2.0560	0.0235	9.5762
300.0000	1.4119	0.1345	3.9553	1.5338	0.0000	6.9010
400.0000	1.1722	0.1070	2.9165	1.2252	0.0000	5.3138
500.0000	1.0167	0.0888	2.2601	1.0165	0.0000	4.2933
650.0000	0.8605	0.0705	1.7154	0.8266	0.0000	3.4025

Published by AIP Publishing on behalf of the National Institute of Standards and Technology.

TABLE 4. (*Continued.*)

Energy (eV)	Elastic ICS ($\times 10^{-16}$ cm^2)	MTCS ($\times 10^{-16}$ cm^2)	Excitation ($\times 10^{-16}$ cm^2)	Direct ionization ICS ($\times 10^{-16}$ cm^2)	Ps formation ($\times 10^{-16}$ cm^2)	Total ($\times 10^{-16}$ cm^2)
850.0000	0.7244	0.0546	1.2318	0.6470	0.0000	2.6032
1000.0000	0.6517	0.0462	1.0026	0.5526	0.0000	2.2069
1500.0000	0.4968	0.0294	0.6042	0.3786	0.0000	1.4796
2000.0000	0.4061	0.0206	0.4123	0.2781	0.0000	1.0964
2500.0000	0.3453	0.0154	0.3047	0.2152	0.0000	0.8652
3000.0000	0.3013	0.0120	0.2369	0.1726	0.0000	0.7108
3500.0000	0.2677	0.0096	0.1909	0.1421	0.0000	0.6006
4000.0000	0.2411	0.0080	0.1578	0.1194	0.0000	0.5183
5000.0000	0.2016	0.0057	0.1140	0.0886	0.0000	0.4043

only our ROP result can be considered further in Sec. 4. The results in Fig. 6(d), for the ionization ICS, are, however, very encouraging. Here, our OP calculation and the CCC result[12] are in very good agreement over their common energy range. Similarly, while our ROP ionization ICS has a slightly lower magnitude than the OP and CCC, in the energy region about the peak of this cross section, its overall accord with the CCC and OP results is actually quite good. As a consequence, in Sec. 4, we anticipate being able to construct a robust recommended ICS dataset for this process.

4. Recommended Data

Based largely on the discussion in Sec. 3, here, we now construct our recommended cross section datasets for positron–Be and positron–Mg scattering in the gas phase.

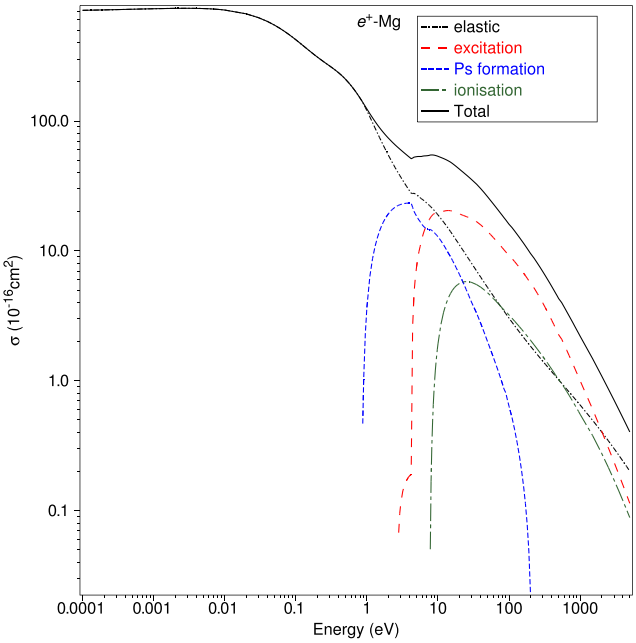

FIG. 4. The present ROP integral and total cross section results for positron scattering from magnesium. See the legend in the figure for the processes considered.

For positron–Be scattering, we form the recommended elastic ICS by taking an average of the Mitroy and Ivanov,[4] Poveda *et al.*,[6] and Reid and Wadehra[5] results up to 0.3 eV and then mapping that onto our OP calculation (scaling factor = 0.946) to extend the results up to 5000 eV. This is effectively the method of Itikawa, who has established a reputation for the critical analysis and forming recommended cross section data in electron–molecule scattering (see, e.g., Refs. 37 and 38). Given the level of accord between the various calculations (see Fig. 5), over their overlapping energy ranges, a conservative estimate of ±20% in the uncertainty of the elastic ICS seems reasonable. In the case of positronium formation, we only have the present ROP and OP results available to form a recommended dataset. Here, our OP calculation ICS does not appear to be correctly trending to the positronium formation energy threshold, and as a result, we simply employ our ROP result as our recommended data. In their recent paper, McEachran and Stauffer[39] found that for positron–helium scattering, their ROP result was, at worst, to within ±25% of the most recent measured cross section from the Australian National University (ANU) group.[40] As a consequence, we adopt an uncertainty of ±25% on our positronium formation ICS in Be. In the case of the sum over all the discrete-excitation electronic-states, we again prefer our ROP result, due to the uncertainty in the correct electronic-state threshold to be applied in our OP computations (see Sec. 2). We do not have a strong guidance here in estimating the uncertainty on those ICSs, and so we opt for a conservative estimate of ±40%. For the recommended ionization ICS, we again apply the Itikawa approach, by taking an average of our OP and ROP results. From 10 eV until threshold, however, to ensure continuity with that average, we use our ROP calculation scaled by a factor of 0.83. In this case, the uncertainty is taken to be the difference between the ROP and OP results, on the one hand, and our recommended ionization ICS on the other hand, which is typically ±25%. Finally, the recommended TCS for positron–Be scattering is simply obtained, at each given incident positron energy, by adding up the elastic ICS, the positronium formation ICS, the ICS for the sum of the discrete-excitation electronic-states, and the ionization ICS. Our estimated uncertainty on these recommended TCS is ±25%. All the Be results from the above process are plotted in Fig. 7(a) and listed in Table 5.

Let us now consider Mg. Remembering that below the positronium formation threshold energy the total cross section is equivalent to the elastic ICS, the recommended TCS of Ratnavelu *et al.*[2] also

Published by AIP Publishing on behalf of the National Institute of Standards and Technology.

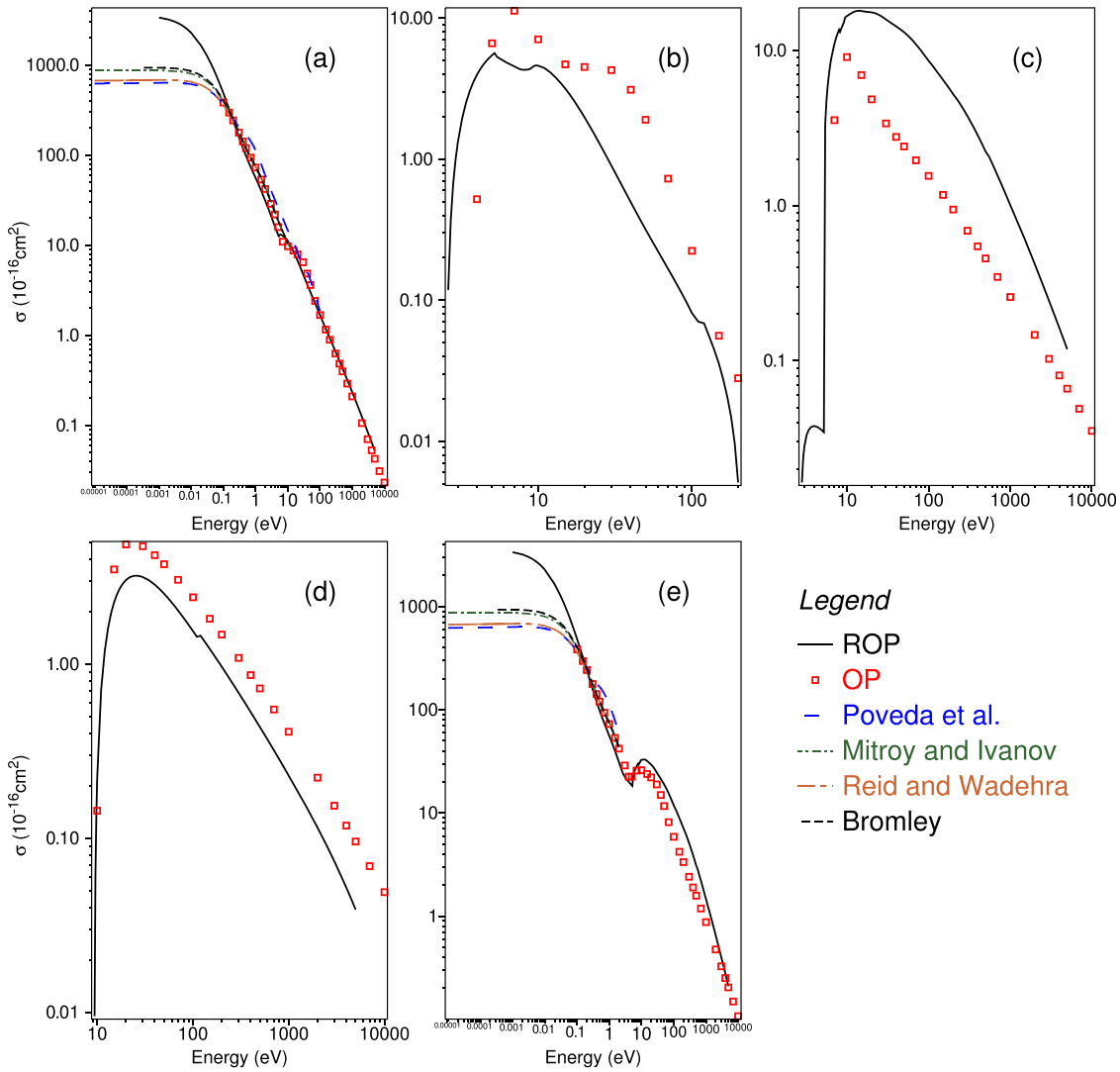

FIG. 5. Comparison of the present OP and ROP integral and total cross section results, against those from earlier studies, for positron–Be scattering. (a) Elastic scattering, (b) positronium formation, (c) sum over discrete electronic-state excitation, (d) ionization, and (e) total scattering. See the legend in the figure and text.

provides a guide to its elastic ICS below E_{Ps}. That comparison suggests that the CCC elastic ICS is quantitatively reproducing this cross section at lower energies. Hence, we base our recommended elastic ICS around the CCC, with an extrapolation to very low energies using the form of the results from Poveda *et al.*[6] (suitably scaled, ×1.33, to map smoothly onto the CCC result) and on extrapolation from 50 eV to 5000 eV by employing our ROP result scaled by a factor of 0.88. We estimate the uncertainty in this data to be ±20%, consistent with Ratnavelu *et al.*[2] for the TCS. Note that the CCC approach for positron–atom scattering was previously shown to provide a good description of the low-energy scattering dynamics by the Trento group,[41–43] with the behavior in Mg being entirely consistent with that observation. For the case of positronium formation, there are several theoretical results available in the literature.[12–15] Of these, the results from the 2-center CCC computation[12] and Gribakin *et al.*[13] are the most comprehensive. We therefore form our recommended Mg positronium formation ICS from an average of the CCC, Gribakin *et al.*,[13] and our ROP results over the energy range where they overlap. At lower energies, we extrapolate to the positronium formation threshold using the ROP computation with a suitable scaling (×1.32) for continuity, while for higher energies (up to 50 eV where the CCC stops), a suitably scaled (×1.13) average of the CCC and ROP results is employed. Beyond 50 eV, the form of the ROP (scaled by ×0.66 for continuity) is used. Given the spread in the available theoretical results [see Fig. 6(b)], for this process, a conservative uncertainty of ±30% is assigned to our recommended positronium formation ICSs. Only the present OP and ROP results are available for the sum over all discrete-excitation electronic state ICSs, and given our earlier

Published by AIP Publishing on behalf of the National Institute of Standards and Technology.

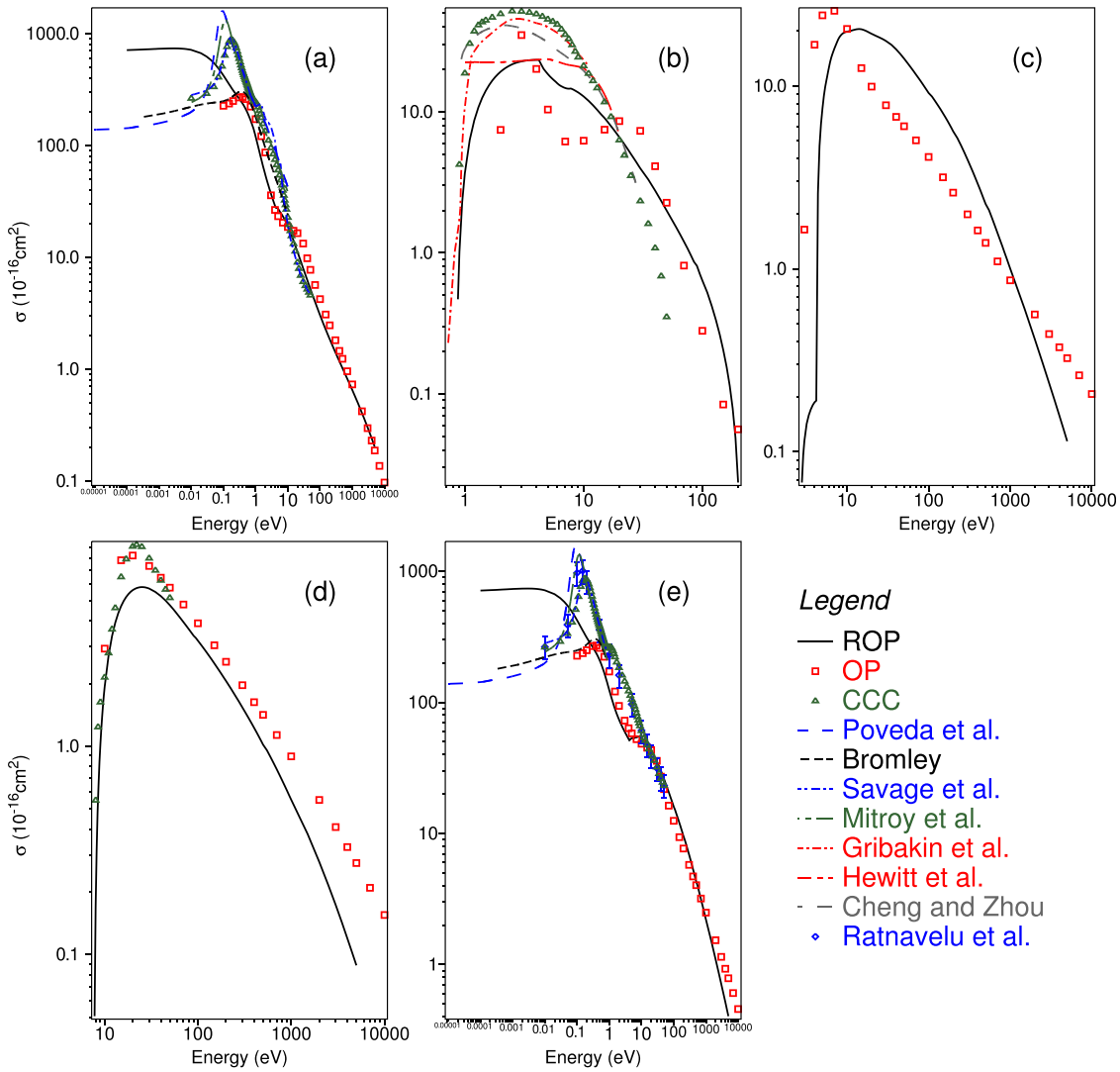

FIG. 6. Comparison of the present OP and ROP integral and total cross section results, against those from earlier studies, for positron–Mg scattering. (a) Elastic scattering, (b) positronium formation, (c) sum over discrete electronic-state excitation, (d) ionization, and (e) total scattering. See also legend in the figure and text.

discussion in Sec. 3 for this process, here we simply adopt the ROP result to be our recommended ICS in Mg. Similar to the case for positron–Be scattering just discussed above, an uncertainty of ±40% is given on these cross sections. Following once again the method of Itikawa,[37,38] for the ionization ICS we take an average of the CCC, OP, and ROP results, up to 50 eV, to form our recommended cross section. Above 50 eV, where the CCC stops, and up to 5000 eV, we employ an average of our OP and ROP results, suitably scaled by a factor of 0.99 to ensure continuity at 50 eV. Note that the ROP result, scaled by 3.37, was employed to extend the ICS down to threshold from 10 eV. In this case, the rather good overall agreement between the three theoretical results enables us to assign a ±20% uncertainty to our recommended ionization ICS. The recommended TCS for positron–Mg scattering is then subsequently determined by simply adding up all the preceding recommended ICSs, with the uncertainty estimate on these data being ±20% (consistent with that from Ratnavelu *et al.*[2]). All the recommended data from this discussion can be found in Table 6, and they are also all plotted in Fig. 7(b).

5. Transport Simulations

While we had previously simulated electron transport behavior for a swarm of electrons in Mg,[23] we had not done so in Be. Therefore, we start this section by looking at the comparative electron transport in Be and Mg, before repeating that discussion but now for positron transport in Be and Mg. We reiterate that these new positron simulations have been undertaken with the recommended positron-Be and positron-Mg cross section database we determined in Sec. 4. We

Published by AIP Publishing on behalf of the National Institute of Standards and Technology.

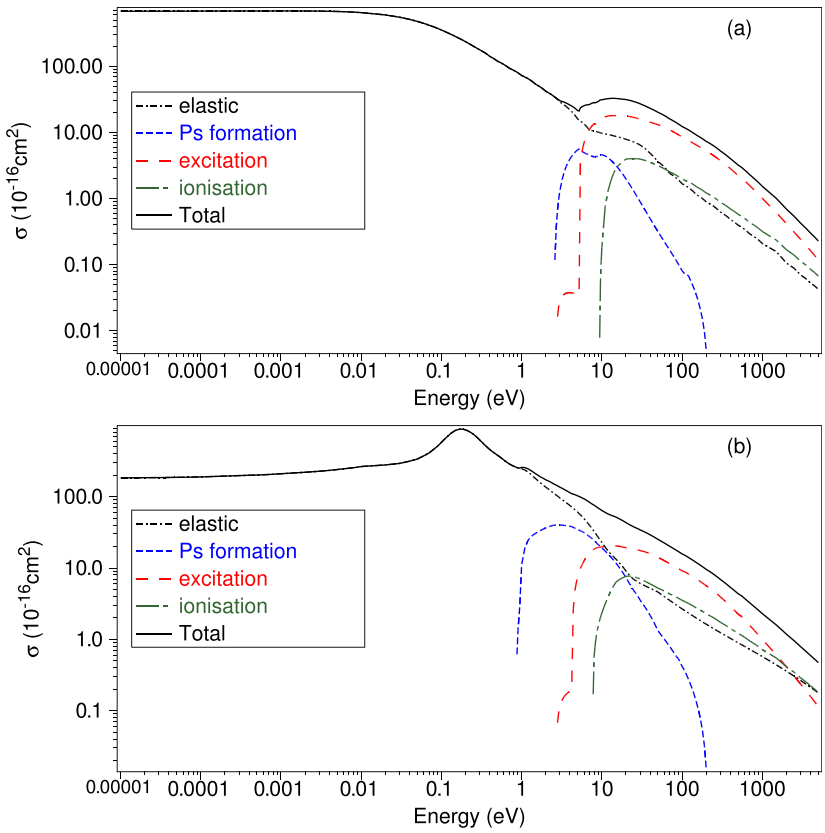

FIG. 7. Recommended integral and total cross sections for positron scattering from (a) Be and (b) Mg. See legend in the figure and text for further details.

highlight that in all calculations for both metal vapors, we have assumed isotropic scattering in the electronic excitation and ionization processes, while we have included the anisotropic nature of elastic scattering through the use of the momentum transfer cross section. The positron elastic MTCS for Be and Mg is implemented directly as per Tables 3 and 4, while for electrons in Be, we have assumed the form of the ROP differential cross section to scale the recommended integral elastic cross section in order to obtain a recommended elastic MTCS. Finally, for each species, a comparison of the positron versus electron transport behavior is presented and discussed. In what follows, we implement a well benchmarked multiterm solution of Boltzmann's equation[44] for the calculation of the transport coefficients in gaseous Be and Mg, and we have found that the two-term approximation[45,46] is generally sufficient for the coefficients presented, over the range of E/n_0 considered. Our physical discussions below will focus on the rates and the drift velocities.

5.1. Electron transport in Be

In Fig. 8, we present the results for the reduced ionization rate k_{io}/n_0, where n_0 is the neutral density, and the bulk and flux drift velocities for an electron swarm in Be vapor over the range of reduced fields, E/n_0, from 0.001 to 1000 Td (1 Td = 10^{21} V m^2). The results are compared with those for electron swarms in Mg vapor[23] at the same temperature of 750 K.

In the low field regime (up to 4 Td), we observe that the flux drift velocity of electrons in Be is substantially higher than that in Mg. This reflects the reduced elastic momentum transfer cross section of Be in the thermal-energy regime (~0.1 eV). This relation is reversed at higher E/n_0 as the elastic momentum transfer rate for electrons in Be substantially increases relative to Mg at the higher energies. This is also reflected in the mean energy (not shown) where the profile for Be lies above that for Mg for the majority of the E/n_0 range considered. At low E/n_0, this is in response to both the reduced elastic and electronic excitation collisional rates for electrons in Be as compared to Mg, while for higher E/n_0, this is impacted upon by the ionization processes. Below 50 Td, the electronic excitation rates for electrons in Be are significantly lower than those in Mg; however, above 50 Td, there is very little difference in these rates. While the threshold for ionization is lower in Be as compared to Mg, the enhanced power input into Be results in the initiation of ionization processes at slightly lower E/n_0 than Mg. The presence of significant ionization manifests itself in differences between the bulk and flux drift velocities at higher E/n_0 (e.g., above a few hundred Td). The ionization process results in the generation of electrons predominantly at the front of the swarm, resulting in a shifting of the center of mass of the swarm in the

Published by AIP Publishing on behalf of the National Institute of Standards and Technology.

TABLE 5. Recommended cross sections for positron scattering from Be. The errors on the elastic ICS are ±20%; ±25% on the positronium formation ICS; an uncertainty of ±40% on the sum of the discrete-excitation electronic-states (inelastic); ±25% on the ionization ICS, and ±25% on the TCS

Energy (eV)	Elastic ICS ($\times 10^{-16}$ cm^2)	Ps formation ($\times 10^{-16}$ cm^2)	Excitation ($\times 10^{-16}$ cm^2)	Direct ionization ICS ($\times 10^{-16}$ cm^2)	Total ($\times 10^{-16}$ cm^2)
1.000000×10^{-5}	680.985	0.000000	0.000000	0.000000	680.985
8.900000×10^{-5}	683.819	0.000000	0.000000	0.000000	683.819
1.000000×10^{-3}	688.764	0.000000	0.000000	0.000000	688.764
2.000000×10^{-2}	598.917	0.000000	0.000000	0.000000	598.917
8.000000×10^{-2}	395.328	0.000000	0.000000	0.000000	395.328
0.160000	271.286	0.000000	0.000000	0.000000	271.286
0.250000	201.686	0.000000	0.000000	0.000000	201.686
0.400000	141.960	0.000000	0.000000	0.000000	141.960
0.700000	93.8000	0.000000	0.000000	0.000000	93.8000
1.20000	65.0720	0.000000	0.000000	0.000000	65.0720
2.60000	34.1040	0.118300	0.000000	0.000000	34.2223
2.70000	32.7880	0.371000	0.000000	0.000000	33.1590
2.80000	31.4720	0.670700	1.640000×10^{-2}	0.000000	32.1591
2.90000	30.1560	0.989800	2.370000×10^{-2}	0.000000	31.1695
3.00000	28.8400	1.31400	2.810000×10^{-2}	0.000000	30.1821
3.40000	26.0848	2.53810	3.590000×10^{-2}	0.000000	28.6588
4.20000	20.7424	4.35360	3.760000×10^{-2}	0.000000	25.1336
5.20000	15.4056	5.65040	3.460000×10^{-2}	0.000000	21.0906
5.40000	14.9072	5.32110	3.32870	0.000000	23.5570
5.60000	14.4088	5.18780	4.77270	0.000000	24.3693
6.20000	12.9136	4.85840	8.00380	0.000000	25.7758
7.00000	10.9200	4.54940	10.9910	0.000000	26.4604
8.00000	10.5187	4.30580	13.6204	0.000000	28.4449
8.20000	10.4384	4.30840	13.1853	0.000000	27.9321
9.40000	9.95680	4.58160	16.2071	7.865861×10^{-3}	30.7534
9.60000	9.87653	4.61190	16.4122	5.125230×10^{-2}	30.9519
9.80000	9.79627	4.61880	16.5771	0.111612	31.1038
10.0000	9.71600	4.60960	16.7163	0.181660	31.2236
13.0000	9.11120	3.79480	17.9754	1.88533	32.7667
15.0000	8.70800	3.16900	17.9675	2.87980	32.7243
20.0000	7.89600	1.98570	17.6137	3.95645	31.4518
26.0000	7.03920	1.20020	16.6850	4.01220	28.9366
30.0000	6.46800	0.898000	15.8581	3.96165	27.1858
35.0000	5.65600	0.653900	14.9840	3.75910	25.0530
40.0000	4.84400	0.496500	14.2927	3.54420	23.1774
45.0000	4.22800	0.391100	13.6935	3.34275	21.6553
50.0000	3.61200	0.317700	13.1214	3.14545	20.1966
60.0000	3.01000	0.223900	12.0010	2.83180	18.0667
70.0000	2.40800	0.167100	10.9566	2.54190	16.0736
80.0000	2.16533	0.129200	10.0366	2.34190	14.6730
100.000	1.68000	8.130000×10^{-2}	8.57160	1.98595	12.3188
110.000	1.57528	7.060000×10^{-2}	8.07670	1.86928	11.5919
120.000	1.47056	6.860000×10^{-2}	7.58590	1.81996	10.9450
130.000	1.36584	5.500000×10^{-2}	7.17030	1.71594	10.3071
150.000	1.15640	3.550000×10^{-2}	6.47730	1.52235	9.19155
170.000	1.05112	2.070000×10^{-2}	5.91390	1.39462	8.38034
190.000	0.945840	9.700000×10^{-3}	5.43910	1.27789	7.67253
200.000	0.893200	5.100000×10^{-3}	5.22690	1.22245	7.34765
300.000	0.627200	0.000000	3.76600	0.885450	5.27865
400.000	0.484400	0.000000	2.84090	0.698550	4.02385
500.000	0.397600	0.000000	2.23150	0.580300	3.20940

Published by AIP Publishing on behalf of the National Institute of Standards and Technology.

TABLE 5. (*Continued.*)

Energy (eV)	Elastic ICS ($\times 10^{-16}$ cm^2)	Ps formation ($\times 10^{-16}$ cm^2)	Excitation ($\times 10^{-16}$ cm^2)	Direct ionization ICS ($\times 10^{-16}$ cm^2)	Total ($\times 10^{-16}$ cm^2)
700.000	0.291200	0.000000	1.56470	0.434650	2.29055
850.000	0.250320	0.000000	1.23640	0.372950	1.85967
1000.00	0.209440	0.000000	1.00980	0.318700	1.53794
1500.00	0.157780	0.000000	0.611900	0.235270	1.00495
2000.00	0.106120	0.000000	0.419200	0.169040	0.694360
2500.00	8.820000×10^{-2}	0.000000	0.310900	0.139400	0.538500
3000.00	7.028000×10^{-2}	0.000000	0.242700	0.113660	0.426640
4000.00	5.292000×10^{-2}	0.000000	0.162800	8.508000×10^{-2}	0.300800
5000.00	4.256000×10^{-2}	0.000000	0.118600	6.733000×10^{-2}	0.228490

direction of the drift velocity and a subsequent enhancement of the bulk drift velocity over the flux drift velocity. Given the near equivalence of the ionization rates for both gases, the modifications to the bulk drift velocity in both gases are also essentially equivalent.

5.2. Positron transport in gaseous Be and Mg

In Fig. 9, we present and compare the results for positron transport in gaseous Mg and Be. There are fundamental differences in the nature of the collisional processes available to positrons (as compared with electrons). First, positronium (Ps) formation is a direct loss-channel for positron swarms. Second, positron-induced ionization is a particle conserving process in contrast to the electron case. While Ps formation can be treated like an attachment process from a transport theory viewpoint, positron-impact ionization requires a different collision operator.[47] There is generally sensitivity in the transport coefficients as to how the excess energy is shared between the scattered positron and ejected electron in an ionization process; however, in the absence of data on this, in what follows, we assume that all fractions of energy sharing are equally likely.

In Fig. 9, for positron transport in Be, we observe that Ps-formation becomes operative at a few Td. In contrast, direct positron impact ionization is observed at a few hundred Td reflecting the substantial difference in the threshold energies for these processes. For the range of E/n_0 considered, the positronium formation rate exceeds the positron-impact direct ionization rate, reflecting the dominance of the Ps-formation cross section over the positron-impact direct ionization cross section in the energy regions up to approximately 15 eV. For sufficiently high E/n_0, we would expect this relation to invert. For positrons in Mg, we observe that Ps-formation is operative at all E/n_0 sampled, indicative of its presence at lower energies and its increased magnitude (which is of an order of magnitude higher) than for Be. Positron impact ionization in Mg is operative at higher E/n_0 than for Be reflecting the slightly lower threshold energy for this process, but more importantly the reduced mean energy for positrons in Mg as compared with Be due to the enhanced elastic and inelastic scattering rates in Mg.

The flux drift velocity for positrons in Be initially increases linearly with E/n_0 before a region of rapid increase in the flux drift velocity (and mean energy—not shown) around 2–6 Td, reflecting the significant decrease in elastic cross section magnitude with energy in this region. The Ps-formation channel then opens which, in turn, modifies the center-of-mass motion of the swarm through selective loss of positrons from the high-energy front of the swarm. This manifests itself in a bulk drift velocity that is less than the flux drift velocity. Indeed, in this field region, the flux drift velocity can be in excess of an order of magnitude greater than the bulk drift velocity. More importantly, a slight negative differential conductivity (NDC—the reduction of drift velocity with increasing E/n_0) emerges over an extended E/n_0 range from 2 Td up to approximately 8 Td. Ps-induced NDC has been predicted for various other gaseous systems including Ar, H_2, and H_2O.[48–50] The mechanism is well understood—as the reduced field increases, the modification to the time rate of change of the center of mass of the positron swarm, brought about by preferential loss of positrons (to positronium) at the front of the swarm, increases at a greater rate than the advective component, and hence, NDC in the bulk then emerges. Similar qualitative behavior is present for positrons in Mg; however, this NDC effect is greatly magnified for positrons in Mg due to the increased magnitude of the associated cross section. The NDC effect is more pronounced here with the bulk drift velocity reducing by over an order of magnitude, with the region for NDC occurring over a much larger range of reduced fields.

5.3. Comparison of electron and positron transport in gaseous Be and Mg

While the scattering channels common to positrons and electrons have distinctly different energy dependencies of their cross sections [the exception to this is for direct ionization scattering where for each species (i.e., either Be or Mg) and above about 100 eV, both our OP and ROP results suggest their cross sections are largely identical], which can be manifestly expressed macroscopically in the field dependence of the transport coefficients, so too can the different processes available to positrons (e.g., positronium formation) over electrons lead to different transport behavior. In Fig. 10, we highlight some important observations on the differences between electron and positron transport in Be and Mg gases.

For Be gas, we observe that the electron drift velocity is approximately an order of magnitude greater than the positron drift velocity at very low E/n_0. Likewise, we observe that the electrons depart from the thermal velocity distribution prior to the positrons (i.e., departure from linear variation with E/n_0) with the mean energy

Published by AIP Publishing on behalf of the National Institute of Standards and Technology.

TABLE 6. Recommended cross sections for positron scattering from Mg. The errors on the elastic ICS are ±20%; ±30% on the positronium formation ICS; an uncertainty of ±40% on the sum of the discrete-excitation electronic-states (inelastic); ±20% on the ionization ICS; and ±20% on the TCS

Energy (eV)	Elastic ICS ($\times 10^{-16}$ cm^2)	Ps formation ($\times 10^{-16}$ cm^2)	Excitation ($\times 10^{-16}$ cm^2)	Direct ionization ICS ($\times 10^{-16}$ cm^2)	Total ($\times 10^{-16}$ cm^2)
1.000000×10^{-5}	183.981	0.000000	0.000000	0.000000	183.981
2.000000×10^{-4}	194.549	0.000000	0.000000	0.000000	194.549
1.000000×10^{-3}	209.769	0.000000	0.000000	0.000000	209.769
1.000000×10^{-2}	264.665	0.000000	0.000000	0.000000	264.665
5.000000×10^{-2}	336.342	0.000000	0.000000	0.000000	336.342
7.000000×10^{-2}	409.715	0.000000	0.000000	0.000000	409.715
0.140000	810.071	0.000000	0.000000	0.000000	810.071
0.170000	888.269	0.000000	0.000000	0.000000	888.269
0.210000	845.020	0.000000	0.000000	0.000000	845.020
0.330000	560.358	0.000000	0.000000	0.000000	560.358
0.450000	414.207	0.000000	0.000000	0.000000	414.207
0.700000	288.537	0.000000	0.000000	0.000000	288.537
0.875000	255.605	0.617463	0.000000	0.000000	256.222
0.900000	251.858	1.33687	0.000000	0.000000	253.195
0.950000	249.199	3.02818	0.000000	0.000000	252.228
1.00000	246.541	11.1265	0.000000	0.000000	257.667
1.10000	236.500	19.2430	0.000000	0.000000	255.743
1.20000	221.549	24.3536	0.000000	0.000000	245.903
1.70000	157.160	33.3589	0.000000	0.000000	190.519
2.00000	135.756	36.6287	0.000000	0.000000	172.385
2.80000	102.059	40.0462	6.780000×10^{-2}	0.000000	142.173
2.90000	98.8625	40.0854	9.550000×10^{-2}	0.000000	139.043
3.20000	91.0475	39.8660	0.142000	0.000000	131.056
3.80000	78.7134	38.9059	0.179600	0.000000	117.799
4.20000	71.9952	38.1249	0.190200	0.000000	110.310
4.40000	68.8814	37.1417	2.58810	0.000000	108.611
4.60000	65.9575	36.2306	4.69740	0.000000	106.885
5.20000	58.0963	33.9728	8.82940	0.000000	100.898
6.40000	45.2680	29.8119	14.2539	0.000000	89.3338
7.80000	33.9246	25.1979	17.9762	0.169973	77.2687
8.00000	32.5581	24.5069	18.3502	0.566464	75.9816
8.60000	29.0637	22.4717	19.1469	1.18134	71.8637
11.0000	19.6689	17.3249	20.0040	3.14575	60.1436
13.0000	15.6264	14.1717	20.4103	4.80101	55.0094
15.0000	13.2930	11.7350	20.4161	6.34267	51.7868
20.0000	9.06761	7.29118	19.2904	7.65800	43.3072
25.0000	6.91139	4.82663	18.3960	7.56110	37.6951
30.0000	6.08586	3.55684	17.6104	7.01875	34.2718
40.0000	5.20545	2.16770	15.8525	5.98839	29.2140
50.0000	4.60955	1.32292	14.1125	5.23107	25.2760
65.0000	3.73636	0.893427	12.0858	4.54869	21.2643
85.0000	3.03568	0.572387	10.2050	3.90210	17.7152
100.000	2.68026	0.422003	9.15150	3.53038	15.7842
120.000	2.34214	0.278045	8.27100	3.19799	14.0892
140.000	2.09508	0.174631	7.44770	2.89871	12.6161
160.000	1.90590	0.102884	6.75630	2.65619	11.4213
180.000	1.75555	5.213755×10^{-2}	6.16250	2.46437	10.4346
190.000	1.69131	3.239550×10^{-2}	5.89550	2.37373	9.99294
200.000	1.63299	1.556839×10^{-2}	5.64600	2.28608	9.58063
300.000	1.24581	0.000000	3.95530	1.73832	6.93943
400.000	1.03431	0.000000	2.91650	1.41786	5.36867
500.000	0.897098	0.000000	2.26010	1.20831	4.36551

Published by AIP Publishing on behalf of the National Institute of Standards and Technology.

TABLE 6. (*Continued.*)

Energy (eV)	Elastic ICS ($\times 10^{-16}$ cm^2)	Ps formation ($\times 10^{-16}$ cm^2)	Excitation ($\times 10^{-16}$ cm^2)	Direct ionization ICS ($\times 10^{-16}$ cm^2)	Total ($\times 10^{-16}$ cm^2)
700.000	0.724155	0.000000	1.56740	0.947113	3.23867
1000.00	0.575036	0.000000	1.00260	0.718774	2.29641
1500.00	0.438358	0.000000	0.604200	0.547358	1.58992
2000.00	0.358327	0.000000	0.412300	0.412482	1.18311
2500.00	0.304680	0.000000	0.304700	0.345715	0.955095
3000.00	0.265856	0.000000	0.236900	0.289041	0.791797
4000.00	0.212738	0.000000	0.157800	0.222224	0.592762
5000.00	0.177884	0.000000	0.114000	0.180603	0.472488

(not shown) of the electrons initially increasing more rapidly with E/n_0 than the positrons. Both of these macroscopic observations reflect the substantially higher elastic MTCS for positrons over electrons for energies well below 0.1 eV. As the reduced field increases further, the mean energy of the positrons increases more rapidly than for electrons due to a combination of a falling positron elastic cross section and the distinct differences in the electronic excitation processes for electrons and positrons. For electrons in Be, the electronic excitation process is operative at lower energies than that for

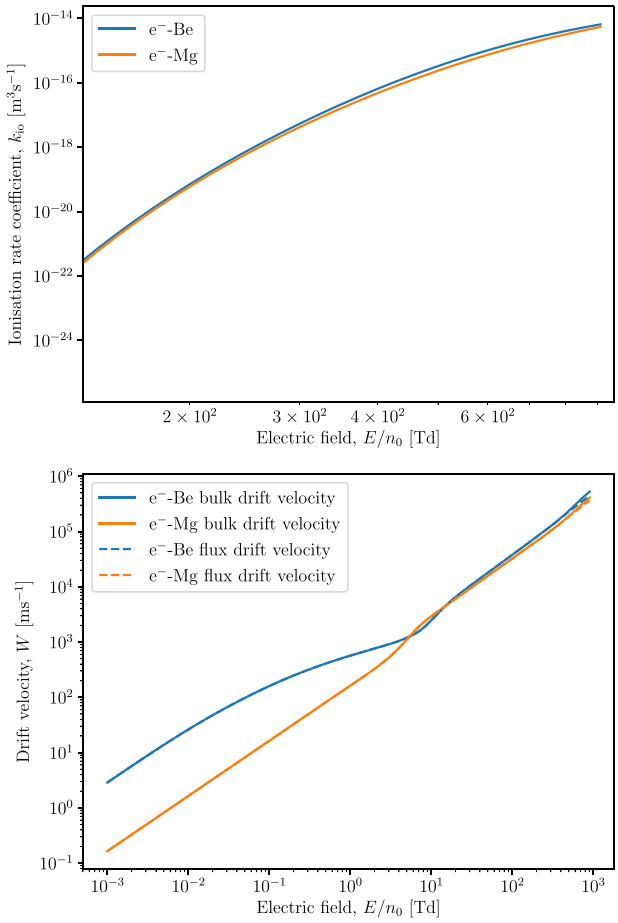

FIG. 8. Comparison of the calculated rate coefficients for ionization (top), bulk (solid), and flux (dashed) drift velocities (bottom) for electrons in Be (blue) and Mg (orange) vapor at 750 K over a range of reduced electric fields. See also the legend for further details.

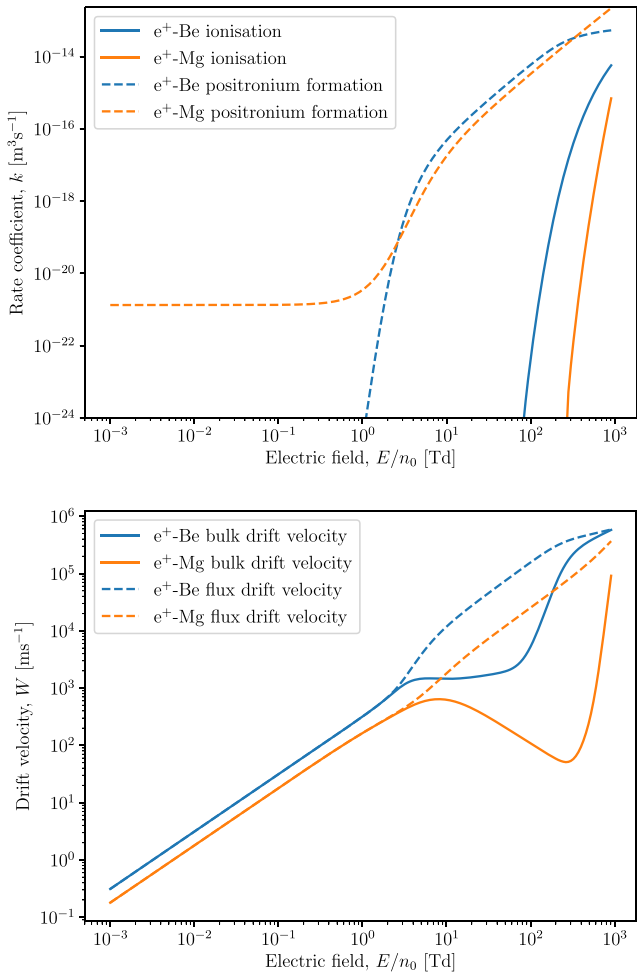

FIG. 9. Comparison of the calculated rate coefficients (top) for ionization (solid) and positronium formation (dashed), bulk (solid) and flux (dashed) drift velocities (bottom) for positrons in Be (blue) and Mg (orange) vapor at 750 K over a range of reduced electric fields. See also the legend for further details.

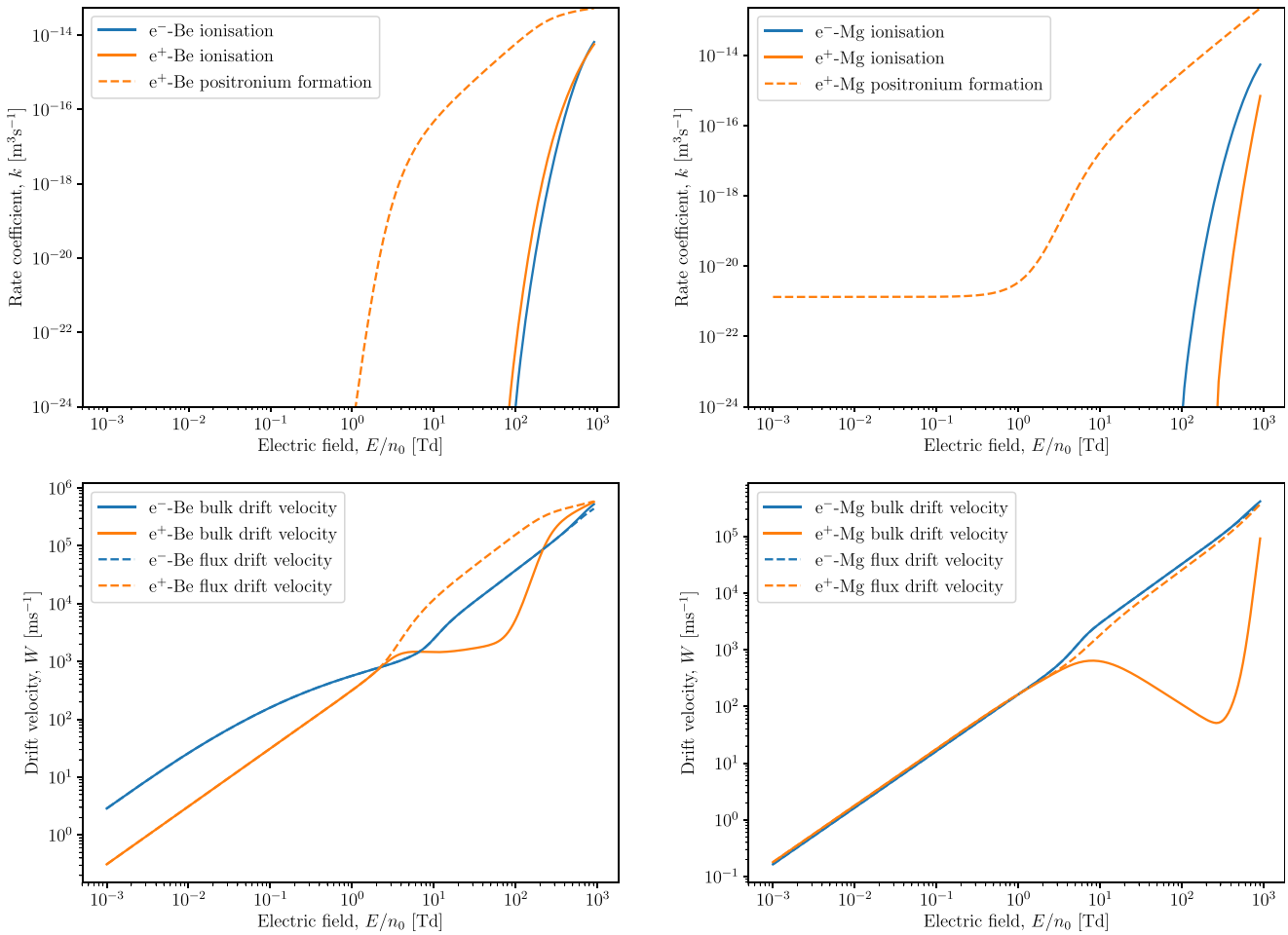

FIG. 10. Comparison of the calculated rate coefficients (top) for ionization (solid) and positronium formation (dashed), bulk (solid) and flux (dashed) drift velocities (bottom row) for electrons (blue) and positrons (orange) in Be (left column) and Mg (right column) vapor at 750 K over a range of reduced electric fields. See also the legend for further details.

positrons, in a nonrelativistic description, with the cross section for electrons being significantly higher in magnitude in the energy range from ~2.6 to 10 eV, above which they are very similar. This mode for absorbing energy from the field for electrons then results in the mean energy of the electrons rising more slowly with E/n_0 than for positrons. The distinctly different nature of the collisional processes is explicitly manifest in the modification to the center-of-mass (or bulk) drift velocity. As detailed above, the Ps-formation process results in a significant decrease in the bulk drift velocity in the region where this channel is significant. Positron-induced ionization does not impact upon the motion of the center of mass since it is a conservative process, in contrast to the case for electron-impact ionization, where the bulk drift velocity lies above the flux drift velocity where this collisional process is significant. For electrons and positrons in Mg, we observe qualitatively similar behaviors though these are magnified given the strength of the Ps-formation process for positrons.

6. Conclusions

We have reported on results from original OP and ROP calculations for positron scattering from beryllium and magnesium. Together with the somewhat limited results from previous work,[2] we were able to use our new computations to construct recommended databases for e^+–Be and e^+–Mg scattering. We have also presented a brief comparative study of the electron and positron transport in Be and Mg gases at 750 K and shown that the transport coefficients are typically distinctly different for the two metal vapors. These differences represent the macroscopic manifestation of differences in the electron and positron cross sections for scattering processes they have in common and, also more importantly, differences in the fundamental nature of the processes available to electrons and positrons. The latter is strikingly highlighted in the effect of the Ps-formation channel which is predicted to generate NDC for positrons in both Be and Mg, yet is predicted to be absent for electrons in both gases. Also, we should highlight that experimental transport measurements for

Published by AIP Publishing on behalf of the National Institute of Standards and Technology.

both these species are highly desirable as they might represent the best opportunity to validate the low-energy cross sections (<0.1 eV) and importantly resonances in these cross sections. This highlights the importance of an accurate and complete set of cross sections for electrons and positrons when modeling their transport in metal vapors, and indeed, the proposed transport measurements also represent an independent method of testing the accuracy and self-consistency of the cross section sets.

Acknowledgments

This work was financially supported, in part, by the Spanish Ministerio de Ciencia, Innovation y Universidades (Project No. FIS2016-80440) and the Australian Research Council (Project Nos. DP160102787, DP180101655, and DP190100696). We thank Dr. L. Campbell for his help with some aspects of this study. Finally, we also thank Professor I. Bray for providing us tables of his CCC data and Dr. M. Bromley for providing us with tables of his results.

7. References

[1]L. Chiari and A. Zecca, Eur. Phys. J. D **68**, 297 (2014).
[2]K. Ratnavelu, M. J. Brunger, and S. J. Buckman, J. Phys. Chem. Ref. Data **48**, 023102 (2019).
[3]M. W. J. Bromley, J. Mitroy, and G. Ryzhikh, J. Phys. B: At., Mol. Opt. Phys. **31**, 4449 (1998).
[4]J. Mitroy and I. A. Ivanov, Phys. Rev. A **65**, 042705 (2002).
[5]D. D. Reid and J. M. Wadehra, J. Phys. B: At., Mol. Opt. Phys. **47**, 225211 (2014).
[6]L. A. Poveda, D. Assafrão, and J. R. Mohallem, Eur. Phys. J. D **70**, 152 (2016).
[7]T. S. Stein, M. Horte, J. Jiang, W. E. Kaupplia, C. K. Kwan, H. Li, and S. Zhou, Nucl. Instrum. Methods B **143**, 68 (1998).
[8]T. S. Stein, J. Jiang, W. E. Kauppila, C. K. Kwan, H. Li, E. Surdutovich, and S. Zhou, Can. J. Phys. **74**, 313 (1996).
[9]E. Surdutovich, M. Horte, W. E. Kauppila, C. K. Kwan, and T. S. Stein, Phys. Rev. A **68**, 022709 (2003).
[10]J. Mitroy, J. Y. Zhang, M. W. J. Bromley, and S. I. Young, Phys. Rev. A **78**, 012715 (2008).
[11]J. S. Savage, D. V. Fursa, and I. Bray, Phys. Rev. A **83**, 062709 (2011).
[12]R. Utamuratov, D. V. Fursa, A. S. Kadyrov, A. V. Lugovskoy, J. S. Savage, and I. Bray, Phys. Rev. A **86**, 062702 (2012).
[13]G. F. Gribakin and W. A. King, Can. J. Phys. **74**, 449 (1996).
[14]R. N. Hewitt, C. Noble, B. H. Bransdon, and C. J. Joachain, Can. J. Phys. **74**, 559 (1996).
[15]C. Chang and Y. Zhou, Phys. Rev. A **73**, 024701 (2006).
[16]C. Makochekanwa, M. Hoshino, H. Kato, O. Sueoka, M. Kimura, and H. Tanaka, Phys. Rev. A **77**, 042717 (2008).
[17]O. Sueoka, C. Makochekanwa, H. Tanina, and M. Kimura, Phys. Rev. A **72**, 042705 (2005).
[18]L. Chiari, A. Zecca, F. Blanco, G. García, and M. J. Brunger, Phys. Rev. A **91**, 012711 (2015).
[19]L. Chiari, A. Zecca, G. García, F. Blanco, and M. J. Brunger, J. Phys. B: At., Mol. Opt. Phys. **46**, 235202 (2013).
[20]A. Zecca, C. Perazzolli, and M. J. Brunger, J. Phys. B: At., Mol. Opt. Phys. **38**, 2079 (2005).
[21]M. J. Brunger, S. J. Buckman, and K. Ratnavelu, J. Phys. Chem. Ref. Data **46**, 023102 (2017).
[22]R. P. McEachran, F. Blanco, G. García, and M. J. Brunger, J. Phys. Chem. Ref. Data **47**, 033103 (2018).
[23]R. P. McEachran, F. Blanco, G. García, P. W. Stokes, R. D. White, and M. J. Brunger, J. Phys. Chem. Ref. Data **47**, 043104 (2018).
[24]D. D. Reid and J. M. Wadehra, J. Phys. B: At., Mol. Opt. Phys. **29**, L127 (1996).
[25]W. Tattersall, L. Chiari, J. R. Machacek, E. Anderson, R. D. White, M. J. Brunger, S. J. Buckman, G. García, F. Blanco, and J. P. Sullivan, J. Chem. Phys. **140**, 044320 (2014).
[26]L. Chiari, A. Zecca, S. Girardi, E. Trainotti, G. García, F. Blanco, R. P. McEachran, and M. J. Brunger, J. Phys. B: At., Mol. Opt. Phys. **45**, 215206 (2012).
[27]R. P. McEachran, D. L. Morgan, A. G. Ryman, and A. D. Stauffer, J. Phys. B: At., Mol. Opt. Phys. **10**, 663 (1977).
[28]A. C. L. Jones, C. Makochekanwa, P. Caradonna, D. S. Slaughter, J. R. Machacek, R. P. McEachran, J. P. Sullivan, S. J. Buckman, A. D. Stauffer, I. Bray, and D. V. Fursa, Phys. Rev. A **83**, 032701 (2011).
[29]F. Blanco, A. M. Roldán, K. Krupa, R. P. McEachran, R. D. White, S. Marjanović, Z. Lj. Petrović, M. J. Brunger, J. R. Machacek, S. J. Buckman, J. P. Sullivan, L. Chiari, P. Limão-Vieira, and G. García, J. Phys. B: At., Mol. Opt. Phys. **49**, 145001 (2016).
[30]S. Chen, R. P. McEachran, and A. D. Stauffer, J. Phys. B: At., Mol. Opt. Phys. **41**, 025201 (2008).
[31]K. Bartschat, R. P. McEachran, and A. D. Stauffer, J. Phys. B: At., Mol. Opt. Phys. **21**, 2789 (1988).
[32]K. Bartschat, R. P. McEachran, and A. D. Stauffer, J. Phys. B: At., Mol. Opt. Phys. **23**, 2349 (1990).
[33]R. P. McEachran, D. L. Morgan, A. G. Ryman, and A. D. Stauffer, J. Phys. B: At., Mol. Opt. Phys. **11**, 951 (1978).
[34]R. P. McEachran and A. D. Stauffer, J. Phys. B: At., Mol. Opt. Phys. **46**, 075203 (2013).
[35]D. D. Reid and J. M. Wadehra, J. Phys. B: At., Mol. Opt. Phys. **30**, 2318 (1997).
[36]D. J. Murtagh, M. Szluinska, J. Moxom, P. Van Reeth, and G. Laricchia, J. Phys. B: At., Mol. Opt. Phys. **38**, 3857 (2005).
[37]Y. Itikawa, J. Phys. Chem. Ref. Data **46**, 043103 (2017).
[38]Y. Itikawa, J. Phys. Chem. Ref. Data **45**, 033106 (2016).
[39]R. P. McEachran and A. D. Stauffer, J. Phys. B **52**, 115203 (2019).
[40]P. Caradonna, A. Jones, C. Makochekanwa, D. S. Slaughter, J. P. Sullivan, S. J. Buckman, I. Bray, and D. V. Fursa, Phys. Rev. A **80**, 032710 (2009).
[41]A. Zecca, L. Chiari, E. Trainotti, D. V. Fursa, I. Bray, and M. J. Brunger, Eur. Phys. J. D **64**, 317 (2011).
[42]A. Zecca, L. Chiari, E. Trainotti, D. V. Fursa, I. Bray, A. Sarkar, S. Chattopadhyay, K. Ratnavelu, and M. J. Brunger, J. Phys. B: At., Mol. Opt. Phys. **45**, 015203 (2012).
[43]A. Zecca, L. Chiari, E. Trainotti, and M. J. Brunger, J. Phys. B: At., Mol. Opt. Phys. **45**, 085203 (2012).
[44]R. D. White, D. Cocks, G. Boyle, M. Casey, N. Garland, D. Konovalov, B. Philippa, P. Stokes, J. de Urquijo, O. González-Magaña, R. P. McEachran, S. J. Buckman, M. J. Brunger, G. Garcia, S. Dujko, and Z. Lj. Petrovic, Plasma Sources Sci. Technol. **27**, 053001 (2018).
[45]G. J. Boyle, W. J. Tattersall, D. G. Cocks, R. P. McEachran, and R. D. White, Plasma Sources Sci. Technol. **26**, 024007 (2017).
[46]R. D. White, R. E. Robson, B. Schmidt, and M. A. Morrison, J. Phys. D: Appl. Phys. **36**, 3125 (2003).
[47]G. J. Boyle, W. J. Tattersall, D. G. Cocks, S. Dujko, and R. D. White, Phys. Rev. A **91**, 052710 (2015).
[48]A. Banković, S. Dujko, R. D. White, J. P. Marler, S. J. Buckman, S. Marjanović, G. Malović, G. García, and Z. Lj. Petrović, New J. Phys. **14**, 035003 (2012).
[49]A. Banković, S. Dujko, R. D. White, S. J. Buckman, and Z. Lj. Petrović, Nucl. Instrum. Methods B **279**, 92 (2012).
[50]M. Šuvakov, Z. L. Petrović, J. P. Marler, S. J. Buckman, R. E. Robson, and G. Malović, New J. Phys. **10**, 053034 (2008).